

Coupled-Channel Calculations for Nuclear Bound States*

E. ROST†

Palmer Physical Laboratory, Princeton University, Princeton, New Jersey

(Received 26 September 1966)

The method of coupled channels is presented for situations where all channels are bound. A numerical relaxation technique is formulated for such problems and is found to be rapid and reliable. Calculations are performed for deformed nuclei (where angular momenta in a rotational band are coupled) and for the Lane isospin $\mathbf{t} \cdot \mathbf{T}$ potential (where proton-nucleus and neutron-analog compositions of a target nucleus are coupled). In either case the relevant radial functions may be used as form factors for the analysis of stripping or pickup experiments. The calculations are applied to (1) deformed components in spherical nuclei (O^{18} and Ca^{40}); (2) a deformed nucleus (Mg^{26}); (3) j -dependent effects in the $1f_{7/2}$ shell; and (4) the extraction of (p,d) spectroscopic factors in the $1f_{7/2}$ shell using the Lane potential. The effect of the channel coupling is found to be important in many instances.

I. INTRODUCTION

THE analysis of nuclear-structure data has shown many instances where the simple central-field potential model¹ is insufficient. A primary example occurs in nuclei far from closed shells where collective degrees of freedom are crucial in understanding the details of the nuclear spectra.² These collective degrees of freedom are strongly coupled to single-particle modes of motion and their effect may often be understood in terms of deformations of the nuclear-potential well (either permanent or vibrational) in which the single-particle orbitals lie. These deformed orbitals are conveniently calculated in a perturbative method which is often quite adequate for describing the energy levels, moments, and other properties of nuclei.^{3,4} However, for nuclear transfer reactions such perturbative calculations fail, even if finite wells are used, since these reactions are highly sensitive to the tail of the radial wave functions which are improperly computed in perturbation expansion. A compromise procedure is often employed⁵ using harmonic-oscillator expansion coefficients and spherical Woods-Saxon radial wave functions, although the accuracy of such a procedure is open to question.

A straightforward method for accurately computing deformed orbitals is available by solving a coupled-channel eigenvalue problem. The eigenvalue can be adjusted to equal the separation energy of the transferred particle in a stripping reaction, i.e., the radial wave function will have the correct tail. Similar coupled-channel eigenvalue problems occur for other

nuclear-structure models and require only a change in the matrix elements and notation. In particular, the Lane isovector potential⁶ $\mathbf{t} \cdot \mathbf{T}$ gives rise to a coupling between nuclear states and their isobaric analog states and an accurate radial wave function may be readily calculated.⁷

In Sec. II a general coupled-channel eigenvalue problem is presented and a relaxation method of solution described. The detailed description of the interaction potential and basis states is given in Sec. III for a permanently deformed nucleus and for the isobaric analog problem. Section IV is devoted to tests of the sensitivity of the approximations and a comparison with alternative procedures. Finally, in Sec. V the radial wave functions are used as form factors in distorted-wave calculations and the results compared with experimental data.

II. GENERAL FORMULATION

The N coupled equations to be considered in this work may be written in the form

$$-\frac{d^2}{dr^2}u_i + F_i u_i + \kappa^2 u_i = \sum_{i'} W_{ii'} u_{i'}, \quad i = 1, 2, \dots, N, \quad (2.1)$$

where F_i and $W_{ii'}$ are known functions of the independent variable r with asymptotic properties

$$\begin{aligned} W_{ii'} &\longrightarrow 0, \\ F_i &\longrightarrow l_i(l_i+1)/r^2 + \eta/r. \end{aligned} \quad (2.2)$$

Here l_i is the orbital angular momentum of the i th component and η is the Coulomb parameter.⁸ (For the analog-state problem an additional constant term appears in the asymptotic form of F_i and may be included in an obvious manner.) Bound solutions

* This work was supported by the U. S. Atomic Energy Commission and the Higgins Scientific Trust Fund. The work made use of the Princeton Computer Facilities, supported in part by the National Science Foundation under Grant No. NSF-GP579.

† Present address: Department of Physics, University of Colorado, Boulder, Colorado.

¹ M. G. Mayer, Phys. Rev. **75**, 1969 (1949).

² A. Bohr, Kgl. Danske Videnskab. Selskab, Mat. Fys. Medd. **26**, No. 14 (1952).

³ S. G. Nilsson, Kgl. Danske Videnskab. Selskab, Mat. Fys. Medd. **29**, No. 16 (1955).

⁴ B. Mottelson and S. G. Nilsson, Kgl. Danske Videnskab. Selskab, Mat. Fys. Skrifter **1**, No. 8 (1959).

⁵ B. Macefield and R. Middleton, Nucl. Phys. **59**, 561 (1964).

⁶ A. M. Lane, Phys. Rev. Letters **8**, 171 (1962); Nucl. Phys. **35**, 676 (1962).

⁷ Similar work has been done independently by T. Tamura (to be published).

⁸ M. Hull and G. Breit, *Encyclopedia of Physics*, edited by S. Flügge (Springer-Verlag, Berlin, 1959), Vol. 41.

(positive κ^2) will thus satisfy

$$u_i \xrightarrow[r \rightarrow \infty]{} H_{l_i}(i\kappa r), \quad (2.3)$$

where $H_l = G_l + iF_l$ denotes the l th Coulombic Hankel function.⁸ The functions $u_i(r)$ must also vanish at $r=0$ since $r^{-1}u(r)$ must be finite, e.g., Eq. (3.6) below. The eigenvalue problem is thus completely specified, κ^2 being the eigenvalue. The usual procedure for solving such a problem would be to guess κ^2 and solve the N equations (2.1) N times, e.g., for each initial guess $(du_i/dr)_0 = \delta_{ii'}$. The solution of the simultaneous equations at a matching radius will yield a mismatch, which may then be reduced by choosing a better value of κ^2 . The disadvantages of this procedure are (1) difficulty in determining *a priori* which of the N solutions one has converged to; (2) the necessity for using a single matching radius independent of i ; (3) computational time proportional to N^2 . A relaxation technique removes the above difficulties and will often converge very rapidly.

Let us therefore start with a "guessed" eigenvalue κ_0^2 and set of functions $u_i^{(0)}(r)$. These are conveniently obtained in terms of solutions with $W_{ii'} = 0$, viz.,

$$u_i^{(0)}(r) = \sum_n c_{ni} v_{ni}(r), \quad (2.4)$$

where $v_{ni}(r)$ satisfy

$$-\frac{d^2}{dr^2} v_{ni} + F_i v_{ni} + k_{ni}^2 v_{ni} = 0, \\ v_{ni}(r) \xrightarrow[r \rightarrow \infty]{} H_{l_i}(ik_{ni}r).$$

Substituting (2.4) into (2.1), one obtains [by multiplying by $v_{ni}(r)$ and integrating] the following system of linear equations:

$$\sum_{n'i'} \mathfrak{M}_{nin'i'} c_{n'i'} = \kappa_0^2 c_{ni}, \\ \mathfrak{M}_{nin'i'} = \int_0^\infty v_{ni}(r) W_{ii'}(r) v_{n'i'}(r) dr + \delta_{ii'} \delta_{nn'} k_{ni}^2. \quad (2.5)$$

For the deformed-well problem, the solutions to (2.5) have been well studied by Nilsson and others^{3,4} and thus are labeled, e.g., by asymptotic quantum numbers, so one does not need to perform many calculations as a function of the coupling strength.

Having obtained⁹ an initial κ_0^2 and $u_i^{(0)}(r)$, one determines an improved set of functions $u_i^{(1)}(r)$ which satisfy uncoupled inhomogeneous equations

$$-\frac{d^2}{dr^2} u_i^{(1)} + F_i u_i^{(1)} + \kappa_0^2 u_i^{(1)} = \sum_{i'} W_{ii'} u_{i'}^{(0)}, \quad (2.6) \\ u_i^{(1)} \xrightarrow[r \rightarrow \infty]{} H_{l_i}(i\kappa_0 r),$$

⁹ The initial guessed functions in (2.4) are improved by first tacking on the correct asymptotic tail (2.6).

except at a matching radius R_i . This radius is chosen near the largest value of r where $d^2 u_i^{(1)}/dr^2 = 0$, i.e., the classical turning point. This choice is important since Eq. (2.6) becomes unstable integrating outwards (inwards) when r is greater (lesser) than R_i . The starting integration values of (2.6) are determined by demanding continuity at $r=R_i$ and $u_i^{(1)}(R_i) = u_i^{(0)}(R_i)$. Near convergence these conditions are satisfied by multiplying the numerical solutions (2.6) appropriately.¹⁰

One can find an improvement to $u_i^{(1)}(r)$ by defining the constants a_i and λ :

$$u_i^{(2)}(r) = a_i u_i^{(1)}(r) \approx u_i(r), \quad (2.7) \\ \kappa^2 = \lambda \kappa_0^2,$$

where a_i is an average scaling factor. Substituting into (2.1) and rearranging gives

$$\left[-\frac{d^2}{dr^2} u_i^{(1)} + F_i u_i^{(1)} + \kappa_0^2 u_i^{(1)} - \sum_{i'} W_{ii'} u_{i'}^{(0)} \right] a_i \\ = (1-\lambda) \kappa_0^2 u_i^{(1)} a_i + \sum_{i'} W_{ii'} (u_{i'}^{(1)} a_{i'} - u_{i'}^{(0)} a_i). \quad (2.8)$$

Now multiplying by $u_i^{(1)}$, integrating from 0 to ∞ , and using (2.6), one arrives at the expression

$$\Delta_i a_i = (1-\lambda) \kappa_0^2 I_i a_i + \sum_{i'} Q_{ii'} a_{i'} - P_i a_i, \quad (2.9)$$

where

$$\Delta_i = \lim_{\epsilon \rightarrow 0} \left| u_i^{(1)} \frac{d}{dr} u_i^{(1)} \right|_{R_i+\epsilon}^{R_i-\epsilon},$$

$$I_i = \int_0^\infty [u_i^{(1)}(r)]^2 dr,$$

$$Q_{ii'} = \int_0^\infty u_i^{(1)}(r) W_{ii'}(r) u_{i'}^{(1)}(r) dr,$$

$$P_i = \sum_{i'} \int_0^\infty u_i^{(1)}(r) W_{ii'}(r) u_{i'}^{(0)}(r) dr.$$

Finally letting $b_i = a_i I_i^{1/2}$ gives

$$\kappa_0^{-2} \sum_{i'} [(I_i I_{i'})^{-1/2} Q_{ii'} - \delta_{ii'} I_i^{-1} (\Delta_i + P_i)] b_{i'} \\ = (\lambda - 1) b_i, \quad (2.10)$$

which is recognized as an eigenvalue equation. If the initial guess is satisfactory the eigenvalue $(\lambda - 1)$ nearest zero gives an improved energy $\kappa_1^2 = \lambda \kappa_0^2$ and the corresponding eigenfunctions b_i give improved solutions to (2.1) $u_i^{(2)} = b_i I_i^{-1/2} u_i^{(1)}$. The cycle is then repeated until sufficient accuracy is obtained. Typically, four or five iterations were sufficient to obtain 5 decimal places in energy and 3 places in the normalization constants. Running time on the IBM 7094 was about 1 min for $N=5$ and increased slightly faster than linearly with N .

¹⁰ Far from convergence, an interpolation procedure is used to get the starting integration values; a detailed description would be out of place here.

III. INTERACTION MODELS

The calculational techniques described in Sec. II are applicable to any situation where a small number of bound channels are needed. An elegant general formula for the radial wave function for a captured particle in a stripping reaction (form factor) has been given by Pinkston and Satchler¹¹ and involves a set of coupled radial equations like (2.1). However, in order to make connection with the data it is necessary to specify the nuclear-structure model in some detail. Only two examples will be given here, the rotational model and the isovector potential model. For later convenience, however, a short discussion of form factors and spectroscopic factors will first be presented.

A. Spectroscopic Factors

In the description of a stripping reaction, one encounters the overlap between final- and initial-nucleus wave functions, integrated over all coordinates except those of the transferred nucleon. This overlap is factored into the product of a spectroscopic amplitude and a normalized single-particle wave function and is written schematically¹¹

$$\int \psi_f^*(\xi, x) \psi_i(\xi) d\xi = (S_{\alpha l_j})^{1/2} \psi_{\alpha l_j}^m(x), \quad (3.1)$$

where $S_{\alpha l_j}$ is the spectroscopic factor for the transition in question. Here we assume that only one single-particle orbital contributes significantly and denote additional quantum numbers by α . The radial part of $\psi(x)$ is called the form factor¹² and is given asymptotically by the separation energy which is simply related to the Q value of the reaction. However the shape of $\psi(x)$ inside the nucleus is affected by the manner in which it is calculated and thus the asymptotic *normalization* is dependent on the interior wave function.

In practice, the form factor is obtained by employing a phenomenological model for $\psi_{\alpha l_j}^m(x)$; in particular, one may use the shell model (letting α label the number of radial nodes) and adjust a central potential to bind $\psi_{\alpha l_j}^m(x)$ correctly. Such a procedure is certainly convenient since it allows extraction of $S_{\alpha l_j}$ in a manner rather independent of the nuclear-structure aspects of the nuclei being studied. However, there exist many situations where this procedure is open to question or overly ambiguous.

A natural generalization occurs if we include more than one channel in computing the form factor. Such a situation occurs naturally for deformed nuclei and is sufficiently flexible to treat several kinds of problems with the same general procedure.

¹¹ W. T. Pinkston and G. R. Satchler, Nucl. Phys. **72**, 641 (1965).

¹² R. H. Bassel, R. M. Drisko, and G. R. Satchler, Oak Ridge National Laboratory Report No. ORNL-3240 (unpublished).

B. Rotational Model

The primary feature of the rotational model is the factorization² of the nuclear wave function into a collective part involving orientation angles and an intrinsic part consisting of appropriate combinations of deformed-well orbitals. This work is primarily concerned with calculating these orbital wave functions with sufficient accuracy so that they may be used in stripping calculations. The intrinsic Hamiltonian involving a single nucleon in a deformed well of A nucleons is taken to be

$$H = -\frac{\hbar^2}{2m} \nabla^2 - \Lambda \left(\frac{\hbar}{2m_p c} \right)^2 \mathbf{L} \cdot \boldsymbol{\sigma} - \frac{1}{r} \frac{d}{dr} V(r) + V(r, \theta). \quad (3.2)$$

Here m is the reduced mass of the nucleon-nucleus system, m_p is the proton mass, and $V(r)$ is a finite well taken to be of the form

$$V(r) = -V_0 [1 + \exp((r - R_0)/a)]^{-1}, \quad (3.3)$$

where $R_0 = r_0(A-1)^{1/3}$ is the nuclear radius and V_0 , r_0 , and a are well parameters to be discussed later. The spin-orbit term in (3.2) is taken to be spherical with a Thomas radial shape and is characterized by a dimensionless strength parameter Λ . The deformed part of the Hamiltonian, $V(r, \theta)$, is generated by deforming equipotentials keeping constant volume. Assuming axially symmetric deformations, one has to second order in β

$$r \rightarrow r_0 [1 + \beta Y_2^0(\theta) - \beta^2/4\pi],$$

$$V(r, \theta) \equiv V(r_0) = V[r/(1 + \beta Y_2^0(\theta) - \beta^2/4\pi)]$$

$$= V(r) + V'(r, \theta),$$

$$V'(r, \theta) = -\beta Y_2^0(\theta) r dV/dr$$

$$+ \beta^2 \left\{ [Y_2^0(\theta)]^2 \left[r^2 \frac{d^2 V}{dr^2} + 2r \frac{dV}{dr} \right] + \frac{1}{4\pi} \frac{dV}{dr} \right\}. \quad (3.4)$$

For charged particles, (3.3) and (3.4) include also the Coulomb potential from a uniform sphere of radius R_0 . In the calculations to be reported, Eq. (3.4) was actually extended to fourth order in β in a straightforward manner, the formulas being given in the Appendix.

The Schrödinger equation $H\chi = E\chi$ can be written

$$\left\{ -\frac{\hbar^2}{2m} \nabla^2 - \Lambda \left(\frac{\hbar}{2m_p c} \right)^2 \mathbf{L} \cdot \boldsymbol{\sigma} - \frac{1}{r} \frac{dV}{dr} + V(r) - E \right\} \chi = -V'(r, \theta) \chi. \quad (3.5)$$

Expanding in spin-angle eigenfunctions

$$\chi = r^{-1} \sum_{\nu j' \Omega'} u_{\nu j' \Omega'}(r) |l' j' \Omega'\rangle, \quad (3.6)$$

substituting into (3.5), and taking the scalar product

with $\langle lj\Omega|$, one obtains the set of coupled equations

$$\left\{ -\frac{\hbar^2}{2m} \left(\frac{d^2}{dr^2} - \frac{l(l+1)}{r^2} \right) - \Delta \left(\frac{\hbar}{2m_p c} \right)^2 \frac{1}{r} \frac{dV}{dr} \left[\begin{array}{c} l \\ -l-1 \end{array} \right] \right. \\ \left. + V(r) - E \right\} u_{lj\Omega}(r) = \sum_{v_j'} K_{lj, v_j'}(r) u_{v_j'\Omega}(r), \\ [j = l \pm \frac{1}{2}] \quad (3.7)$$

which is seen to be of the form of (2.1). The coupling term is

$$K_{lj, v_j'}(r) = -\langle lj\Omega | V'(r, \theta) | l' j' \Omega \rangle, \quad (3.8)$$

which may readily be evaluated explicitly using (3.4) or (A4) and is seen to be surface peaked. The projection quantum number Ω is a constant of the motion. Equation (3.7) is the same as a simple potential-well equation in the case of a single lj channel since then the coupling term $K^{\Omega}(r)$ is equivalent to a change in the potential shape. For more than one channel, however, effects due to the coupling may be significant, especially for weak lj channels.

In the rotational model the nuclear wave function in the space fixed frame is given in the simplest case by $\psi_m^j = D_{m\Omega}^j(\theta_i) \chi_{\Omega}$, where θ_i denote Euler angles connecting body and space axes. The model outlined above further assumes negligible rotational energy, i.e., all members of a band have the same energy. It is possible to generalize (3.7) so that the energy depends on j but the significance of such a procedure would be questionable. The crucial point of the analysis is that *all* components of χ have the asymptotic form

$$u_{lj\Omega}(r) \xrightarrow[r \rightarrow \infty]{} H_l(ikr), \quad (3.9) \\ \hbar^2 \kappa^2 / 2m = B \equiv -E,$$

i.e., they have the correct tail for a stripping form factor for a captured particle of angular momentum l with separation energy B . The connection between the stripping form factors and the differential cross section is thoroughly treated by Satchler.¹³ In this work we ignore coupling effects on the distorted entrance and exit channels in calculating differential cross sections.

C. Isovector-Potential Model

The isovector potential $(V_1/A)\mathbf{t} \cdot \mathbf{T}$ was introduced by Lane⁶ to explain analog-state (p, n) reactions¹⁴ in terms of a quasi-scattering process in which charge is exchanged by this potential. In the simplest approximation, only a single spherical orbital need be considered, in which case the generalized Hamiltonian for

relative motion may be written as

$$H = -\frac{\hbar^2}{2m} \nabla^2 + V_0(r) + \frac{V_1(r)}{A} \mathbf{t} \cdot \mathbf{T} \\ + \left(\frac{1}{2} - t_z \right) (V_C(r) - \Delta_C). \quad (3.10)$$

The Coulomb energy is denoted by Δ_C and lower-case \mathbf{t} implies operation on nucleon charge coordinates. The total wave function for the two-channel system is of the form¹⁵

$$\psi = r^{-1} \{ u_p(r) | pC \rangle + u_n(r) | nA \rangle \}, \quad (3.11)$$

where the kets $| pC \rangle$ and $| nA \rangle$ denote the spin, angle, and charge quantum number of each component. The (daughter) nucleus A is the analog of the ground state of nucleus C , i.e., $A = T_C$. If we assume that nucleus C with N neutrons and Z protons has good isospin $T_0 \equiv \frac{1}{2}(N - Z)$, as is reasonable for low-lying states in nuclei, substitution of (3.11) into the Schrödinger equation yields the coupled equation

$$\left(H_0 - \frac{V_1(r)}{A} \frac{T_0}{2} + V_C(r) - \Delta_C - E_n \right) u_p(r) \\ = -\frac{V_1(r)}{A} \left(\frac{T_0}{2} \right)^{1/2} u_n(r), \\ \left(H_0 + \frac{V_1(r)}{A} \frac{T_0 - 1}{2} - E_n \right) u_n(r) \\ = -\frac{V_1(r)}{A} \left(\frac{T_0}{2} \right)^{1/2} u_p(r), \quad (3.12)$$

where

$$H_0 \equiv -\frac{\hbar^2}{2m} \left(\frac{d^2}{dr^2} - \frac{l(l+1)}{r^2} \right) + V_0(r)$$

and $V_0(r)$ is a central plus spin-orbit potential term. Equation (3.12) is readily applied to the quasi-elastic (p, n) process in which case the eigenenergy E_n is positive.

Equation (3.12) may also have negative-energy solutions in which case it has a form similar to that discussed in Sec. II.¹⁶ In general, two solutions will be found for (3.12) corresponding approximately to coupled isospin $T_0 - \frac{1}{2}$ and $T_0 + \frac{1}{2}$. The goodness of isospin can then be investigated in this model by solving (3.12) numerically. The lower energy ($T \approx T_0 - \frac{1}{2}$) solution corresponds in this model to the lowest state of ψ , i.e., the target state in a pickup reaction. In a proton-pickup experiment one thus reaches the unique state C

¹³ G. R. Satchler, Ann. Phys. (N. Y.) 3, 275 (1958).

¹⁴ J. D. Anderson and C. Wong, Phys. Rev. Letters 7, 250 (1961).

¹⁵ D. Robson, Phys. Rev. 137, B535 (1965).

¹⁶ The Δ_C term in the proton channel is included with F_i and the boundary condition (2.3) is appropriately modified for this channel.

with $T=T_0$. For the neutron-pickup experiment, however, one reaches not only the analog state $A(T=T_0, T_z=T_0-1)$ but also a lower lying configuration state¹⁷ ($T=T_0-1, T_z=T_0-1$). Thus if one is dealing with a target having n_p protons and n_n neutrons of a given configuration, the summed spectroscopic factor for proton pickup is n_p and one immediately obtains¹⁸ the neutron-pickup spectroscopic factors to analog and configuration states

$$S_{\text{analog}} = n_p \int_0^\infty u_n^2 dr / \int_0^\infty u_p^2 dr \approx n_p \frac{1}{2T_0}, \quad (3.13)$$

$$S_{\text{config}} = n_n - S_{\text{analog}}.$$

The approximate strength ratio of neutron and proton components is a simple ratio of vector coupling coefficients for forming good $T_0 - \frac{1}{2}$ isospin.¹⁹ The comparison of these predictions to (p,d) data in the $1f_{7/2}$ shell will be discussed in Sec. V. It will be demonstrated there that the extraction of the spectroscopic factor depends rather strongly on how the form factor $u_n(r)$ is calculated.

IV. STUDIES OF THE MODEL

The reliability and accuracy of the model described in the preceding sections will now be investigated for several specific cases. It is therefore necessary to specify well parameters (r_0, a, Λ, V) for Eq. (3.3). To a large extent these may be determined by fitting single-particle level position in spherical nuclei and also by optical-model analysis of elastic proton scattering. An average optical-model (OM) set follows the work of Perey²⁰ and is $r_0=1.25$ F, $a=0.65$ F, and $\Lambda=25$. The well depth is adjustable and we have chosen $V=55$ MeV as a reasonable value for light nuclei. An alternative set of well parameters comes from the analysis of Ross, Mark, and Lawson (RML),²¹ who fitted many level positions in magic nuclei. Their parameters are $r_0=1.30$ F, $a=0.69$ F, $\Lambda=39.5$, and $V=42.8$ MeV and refer to neutron levels; for protons a larger V is needed.

The effect of the well parameters is investigated in Fig. 1 for the $A \sim 40$ region where OM and RML sets are compared. Also shown in the figure are energy levels for a harmonic-oscillator well, i.e., Nilsson levels, using the original parameters of Nilsson.³ Except for a change of origin, one sees no violent effects though there are differences in detail, especially for the weaker bound RML levels. Such binding effects are especially

¹⁷ In practice, several configuration states are seen, so we refer to their summed strength.

¹⁸ J. B. French and M. H. Macfarlane, Nucl. Phys. **26**, 168 (1961).

¹⁹ This derivation of the sum rules is essentially that of B. F. Bayman, in Proceedings of the Conference on Isobaric Spin, Tallahassee, 1966 (unpublished).

²⁰ F. G. Perey, Phys. Rev. **131**, 745 (1963).

²¹ A. A. Ross, H. Mark, and R. D. Lawson, Phys. Rev. **102**, 1613 (1956).

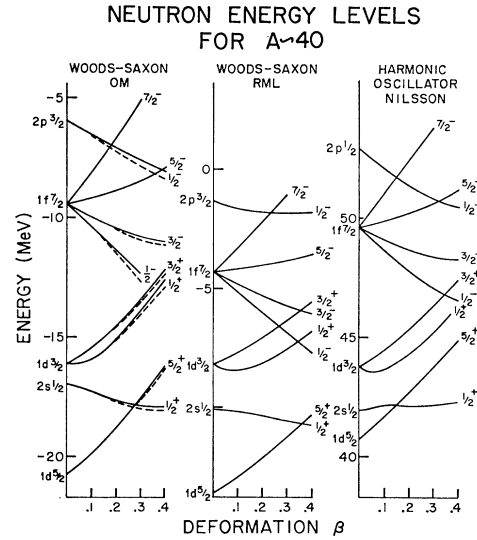


Fig. 1. Single-particle energy levels for neutrons in the $A \sim 40$ region. OM parameters are $r_0=1.25$ F, $a=0.65$ F, $\Lambda=25$, $V=55$ MeV; RML parameters are $r_0=1.30$ F, $a=0.69$ F, $\Lambda=39.5$, $V=42.8$ MeV; Nilsson parameters (Ref. 3) are $\kappa=0.05$, $\mu=0$ ($N=0, 1, 2$), $\mu=0.35$ ($N=3$), $\hbar\omega_0=12$ MeV. The dashed lines in the OM curves were computed with coupled channels; the solid lines with perturbation theory. In all cases the basis consisted of the spherical levels $1s_{1/2}$, $1d_{5/2}$, $2s_{1/2}$, $1d_{3/2}$ (even parity) and $1p_{3/2}$, $1p_{1/2}$, $1f_{7/2}$, $2p_{3/2}$, $1f_{5/2}$, $2p_{1/2}$ (odd parity).

important on the wave functions and will be investigated later. Since the levels of a finite-well calculation depend on the mass region, it was decided not to attempt a general tabulation here.²²

The effect of performing the complete coupled-channels calculation is also shown in Fig. 1 for the OM finite-well parameters and is seen to be quite small—less than 1% as measured from the bottom of the well. Even for heavy nuclei, the perturbation estimate is quite good for obtaining single-particle energies. (However, it may not be satisfactory for computing equilibrium deformations.) The effect of truncating the expansion in (3.4) was also studied by “turning off” the β^3 and β^4 terms. The largest effects (for $\Omega=\frac{1}{2}$ and large deformation) were found to be unimportant even in the wave functions. Thus in this region, at least, the expansion in deformation parameter β is converging.

We turn now to the calculation of the radial wave functions. The exact intrinsic function was expanded in spin-angle eigenfunctions

$$\chi_\Omega = r^{-1} \sum_{ij} u_{ij\Omega}(r) |lj\Omega\rangle \quad (4.1)$$

for a deformed orbital with angular-momentum projection Ω . Note that the radial components $u_{ij\Omega}(r)$ depend on Ω and are *not* normalized to unity. The per-

²² Partial tabulations using perturbation theory are given by R. H. Lemmer and A. E. S. Green [Phys. Rev. **119**, 1043 (1960)] and by A. Faessler and R. K. Sheline [*ibid.* **143**, 1003 (1966)].

TABLE I. Coefficients c_{lj}^2 of a perturbation treatment compared with normalizations of a coupled-channels treatment. Well parameters OM are employed for $A \sim 40$ and $\beta = 0.3$ (see Fig. 1).

Level		Perturbation c_{nlj}^2						Coupled channels $\int u^2 dr$			
Ω	E (MeV)	$1s_{1/2}$	$2s_{1/2}$	$1d_{3/2}$	$1d_{5/2}$			$s_{1/2}$	$d_{3/2}$	$d_{5/2}$	
$\frac{1}{2}^+$	-18.00	0.000	0.209	0.656	0.135			0.214	0.624	0.162	
$\frac{3}{2}^+$	-17.69	1.00			1.00	
$\frac{1}{2}^+$	-14.14	0.003	0.619	0.312	0.066			0.591	0.336	0.073	
$\frac{3}{2}^+$	-13.58	0.959	0.041			...	0.960	0.040	
		$1p_{1/2}$	$1p_{3/2}$	$2p_{1/2}$	$2p_{3/2}$	$1f_{5/2}$	$1f_{7/2}$	$p_{1/2}$	$p_{3/2}$	$f_{5/2}$	$f_{7/2}$
$\frac{1}{2}^-$	-12.61	0.000	0.016	0.022	0.276	0.008	0.678	0.028	0.312	0.011	0.649
$\frac{3}{2}^-$	-10.89	...	0.008	...	0.114	0.016	0.862	...	0.127	0.018	0.855
$\frac{5}{2}^-$	-8.45	0.017	0.983	0.016	0.984
$\frac{1}{2}^-$	-7.87	0.005	0.000	0.343	0.263	0.162	0.227	0.341	0.238	0.166	0.255
$\frac{3}{2}^-$	-5.15	1.00	1.00

turbation expression, on the other hand, can be written

$$x_{\Omega}(\text{pert}) = r^{-1} \sum_{lj} c_{lj}(\Omega) v_{lj}(r) |lj\Omega\rangle, \quad (4.2)$$

where $v_{lj}(r)$ are normalized to unity and are independent of Ω . The $c_{lj}(\Omega)$ coefficients give the amplitude of the lj term (an extra index n should be added if spherical orbitals differing only in number of radial nodes are included). The square of these coefficients is thus comparable to the integral

$$\int_0^{\infty} [u_{lj\Omega}(r)]^2 dr.$$

Such a comparison is presented in Table I for the OM case of Fig. 1 with $\beta = 0.3$. It is seen that some noticeable changes are present; for larger A when several neighboring spherical levels of the same parity occur, much larger effects are seen in the relative normalizations.

The primary difference between the wave functions in (4.1) and (4.2), however, is not in the component normalization but is in the radial shape, especially near the nuclear surface where the coupling term in (3.7) is large. A typical example is shown in Fig. 2 for the $d_{3/2}$ component of the highest $\frac{1}{2}^+$ level in Fig. 1. In the critical surface region, the exact coupled-channel wave

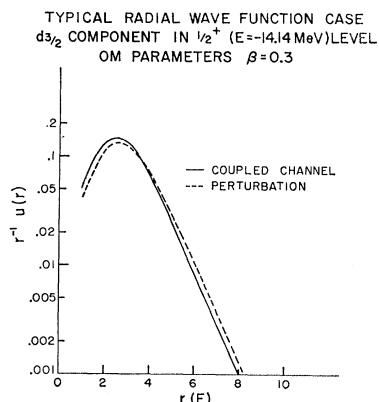


FIG. 2. Comparison of coupled channels and perturbation calculations of a radial wave function for a typical case.

function is about 15% smaller than the perturbation wave function, thus causing a 30% effect in a cross section sensitive to this region.

In order to examine the radial effect closely it is instructive to consider an extreme example. A useful case is the $g_{9/2}$ component in a $2s, 1d$ nucleus, say Mg^{25} , which occurs in this model via $\Delta N = 2$ admixture due to deformation. Picking a "reasonable" deformation $\beta = 0.4$, assuming an $\Omega = \frac{5}{2}$ band, and using OM parameters,²³ one obtains the wave functions displayed in Fig. 3. In this case the amplitude of the $g_{9/2}$ component was only about 1% of the total, so that the coupling terms dominate; indeed $g_{9/2}$ is unbound in any reasonable spherical well in this mass region. Figure 3 shows two attempts to circumvent this fact and still use perturbation theory: (1) by employing a resonant boundary condition for $g_{9/2}$, normalizing the interior, and proceeding as before, and (2) by using an unreasonable well of large radius combined with the perturbation amplitude c_{lj} computed with method (1). Neither attempt is satisfactory in this extreme situation.

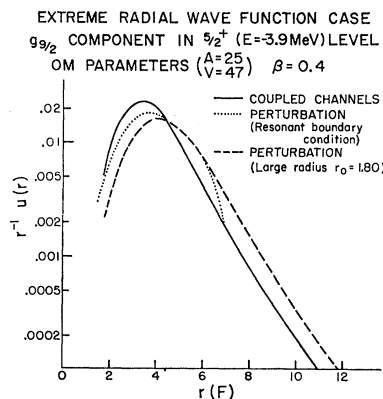


FIG. 3. Comparison of coupled channels and perturbation calculations of a radial wave function for an extreme case.

²³ The well depth was taken to be $V = 47$ MeV in order to fit the experimental separation energies.

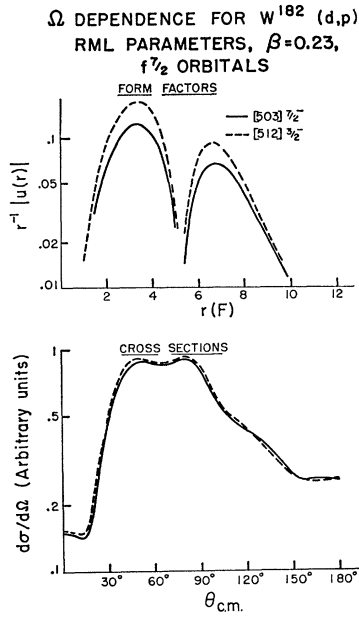


FIG. 4. Form factors and DW cross sections for the $W^{182}(d,p)W^{183}$ reaction at 12 MeV. The $f_{7/2}$ orbitals were computed in a deformed well with $\Omega = \frac{7}{2}^-$ (solid curve) and $\Omega = \frac{3}{2}^-$ (dashed curve). The well depths (RML parameters) were adjusted to fit the approximately equal separation energies as determined in Ref. 24. Optical parameters for the DW calculations were taken to be the measured D2P1 set of Ref. 25.

Since the radial wave functions in (4.1) depend on Ω , one might expect to observe an effect on the stripping cross section, i.e., an Ω dependence. This feature is investigated in Fig. 4, where the $f_{7/2}$ components of the $\frac{3}{2}^-$ and $\frac{7}{2}^-$ band²⁴ in W^{183} (asymptotic quantum numbers⁴ [512] and [503]) are studied using RML parameters and $\beta=0.23$. The [503] $\frac{7}{2}^-$ is largely ($\sim 90\%$) composed of $f_{7/2}$ and thus the extracted $f_{7/2}$ wave function resembles a simple spherical one; the [512] $\frac{3}{2}^-$ band, however, has only 10% $f_{7/2}$ strength, the remainder being largely $f_{5/2}$ and $h_{9/2}$. As may be seen from the figure, an effect is present on the form factors which for display purposes are equated asymptotically and plotted semilogarithmically. The distorted-wave (DW) calculations for the 12-MeV deuteron stripping experiment used the measured optical parameters of Siemssen and Erskine.²⁵ Only a very small effect is seen which reflects the overwhelming dominance of the tail region for this reaction. A hint of such dependence appears in the stripping data²⁵ but the DW analysis is not reliable enough for such fine detail. Higher energy experiments would be needed to verify band dependence in the stripping angular distributions.

Finally, we turn to the analog-state problem treated by the coupled equation in (3.12). In the limit of good isospin, the radial functions in (3.11) are proportional and thus one may write immediately¹⁵ for the target wave function

$$\psi = r^{-1}v(r)(2T_0+1)^{-1/2}\{(2T_0)^{1/2}|pC\rangle - |nA\rangle\}, \quad (4.3)$$

where the radial function $v(r)$ is normalized to unity. The accuracy of (4.3) is tested in Fig. 5 and Table II

TABLE II. Relative normalizations of neutron and proton channels for the Fe (target) isotopes.

C	A	T_0	r_0	B	$1/2T_0$	$\int u_n^2 dr / \int u_p^2 dr$
Mn ⁵³	Fe ⁵³	$\frac{3}{2}^-$	1.270	17.66	0.333	0.337
Mn ⁵⁵	Fe ⁵⁵	$\frac{3}{2}^-$	1.280	18.98	0.200	0.208
Mn ⁵⁷	Fe ⁵⁷	$\frac{3}{2}^-$	1.291	20.47	0.141	0.150

for the iron (target) isotopes using OM well parameters, the radii being adjusted slightly to fit the experimental separation energies. The coupling term was taken to be of surface form [see Eq. (5.4)] with $V_1=100$ MeV. It is seen from the table that the relative normalizations agree with the isospin formula to about 5% with the percentage inaccuracy increasing as one increases T_0 . For higher T_0 , the relative inaccuracy of the $1/2T_0$ ratio might be serious in some applications. However, the overlap with good isospin is about 99%, a fact which lends credibility to the initial assumption of the model.

V. COMPARISONS WITH EXPERIMENT

In this section the bound-state wave functions will be used as form factors for DW calculations and the predicted cross sections compared to experimental data. A limited selection is taken in order to illustrate the applications of the model.

A. $O^{18}(He^3,d)F^{19}$

A reanalysis of the $O^{18}(He^3,d)F^{19}$ reaction²⁶ to the first three states of F^{19} has been published elsewhere.²⁷ Briefly, it was found that deformed-well radial wave functions were significantly larger in the crucial surface region than spherical-well wave functions for the positive-parity levels of F^{19} . Therefore the use of deformed-well functions in the DW analysis yielded smaller spectroscopic factors for positive parity levels and hence a larger O^{18} core-excitation probability as measured by the relative odd-parity yield. The effect is shown in Fig. 6 for the $d_{5/2}$ component of the $\frac{1}{2}^+$

ANALOG DAUGHTER WAVE FUNCTIONS ($T_0 = \frac{3}{2}$) FOR Fe^{56} TARGET

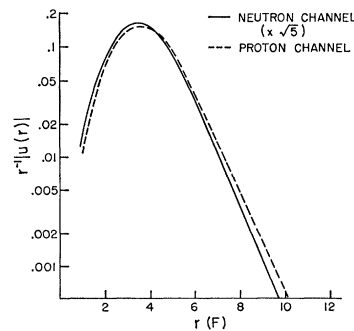


FIG. 5. Comparison of radial wave functions for $T_0 = \frac{3}{2}$ daughter-plus-nucleon system. Well parameters are $r_0=1.28$ F, $a=0.65$ F, $\Lambda=25$, $V=55$ MeV plus a Lane symmetry-energy term of surface form, Eq. (5.4), with $V_1=100$ MeV.

²⁴ J. R. Erskine, Phys. Rev. **138**, B66 (1965).

²⁵ R. H. Siemssen and J. R. Erskine, Phys. Rev. **146**, 911 (1966).

²⁶ J. R. Erskine, R. E. Holland, R. D. Lawson, M. H. Macfarlane, and J. P. Schiffer, Phys. Rev. Letters **14**, 915 (1965).

²⁷ E. Rost, Phys. Letters **21**, 87 (1966).

TABLE III. Extracted distorted-wave results for Mg²⁵.

Ω	j	E _x (MeV)	dσ/dΩ (mb/sr)	Spherical extraction				Deformed extraction			
				V (MeV)	σ _{DW} (mb/sr)	c _{ij} ² (ex)	c _{ij} ² (th) (Nilsson)	V (MeV)	σ _{DW} (mb/sr)	c _{ij} ² (ex)	c _{ij} ² (th) (∫u ² dr)
5/2 ⁺	5/2	0	3.98	47.0	3.08	0.65	1.00	53.6	2.58	0.77	0.99
1/2 ⁺	1/2	0.58	2.58	50.5	6.86	0.19 ^a	0.11	50.1	7.88	0.17 ^a	0.28
3/2 ⁺	3/2	0.98	2.15	55.2	2.74	0.39	0.61	49.3	4.57	0.23	0.46
(9/2 ⁺)	(9/2)	(1.61)	(0.10)	>100				49.7	~0.9	~0.16	~0.002
5/2 ⁺	5/2	1.96	1.15	43.6	3.86	0.15	0.27	47.5	2.68	0.21	0.26
1/2 ⁺	1/2	2.56	0.85	46.4	7.02	0.061 ^a	0.56	54.9	6.51	0.065 ^a	0.47
3/2 ⁺	3/2	2.80	3.05	51.7	3.75	0.41	0.31	54.4	3.15	0.49	0.47
5/2 ⁺	5/2	3.40	small	86.8	0.508	≤0.04 ^b		47.0	0.957	≤0.02 ^b	0.014
1/2 ⁻	1/2	3.40	5.66	66.9	6.54	0.43	0.58	52.2	6.57	0.43	0.55

^a DW fits are very poor.

^b An experimental value dσ/dΩ=0.04 mb/sr was assumed. This is the measured 25° cross section for the (9/2⁺) level at 4.055 MeV.

ground-state band of F¹⁹. The OM parameters are reasonable in this region and do very well for spherical F¹⁷ with V~54 MeV. Using the same well to bind F¹⁹ with the experimental separation energy requires β=0.5, a reasonable value for such a light nucleus. Obtaining the additional binding by deepening the well, however, underestimates the tail region significantly.

B. Mg²⁴(d,p)Mg²⁵

The structure of Mg²⁵ was investigated by Čujec²⁸ with 15-MeV deuterons. Spectroscopic factors were extracted from the stripping differential cross sections using a DW analysis with spherical-well wave functions (depth varied to fit separation energy) and compared to the Nilsson harmonic-oscillator coefficients.³ The relevant levels and their band structure are shown in Fig. 7 (these bands are the lowest three plotted in Fig. 1). It seemed worthwhile to repeat the calculation using deformed-well radial wave functions for the form factors in the DW calculations. The optical parameters were taken to be the same as those used by Čujec²⁸ and the fits to the angular distributions were found to be similar (i.e., poor fits for l=0). The nuclear-structure

information was extracted using the formula given by Satchler¹³:

$$d\sigma(\theta)/d\Omega = 2c_{ij}^2\sigma_{DW}(\theta), \tag{5.1}$$

where σ_{DW} is the computed distorted-wave cross section using a normalized (spherical or deformed) form factor.²⁹ The results obtained by equating (5.1) at θ=25° are presented in Table III. In obtaining the deformed levels β=0.4 was assumed and the depth of the OM well was adjusted to yield correct separation energies. This adjustment was appreciable since the rotational energies are large. Despite this limitation, a smaller spread is seen in V especially for the "unusual" levels at 3.40 MeV.

The agreement between the extracted c_{ij}² values and the normalization integral, i.e., the prediction of the rotational model, are quite adequate except for the 1/2⁺ level at 2.56 MeV. This is brought into line by using a smaller β~0.2 or by invoking considerable band mixing. Neither alternative is particularly disturbing for such a light nucleus.

Of particular interest are the ill-observed l=4 tran-

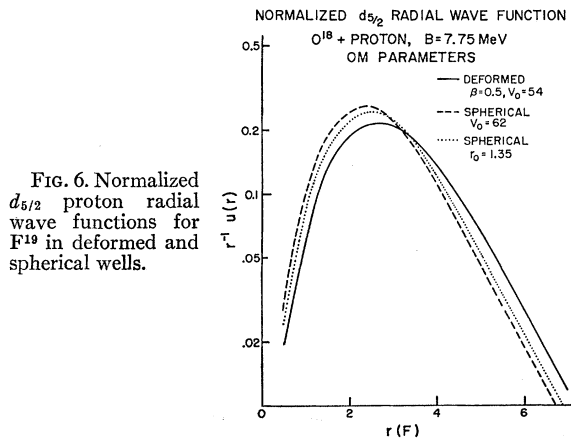


FIG. 6. Normalized d_{5/2} proton radial wave functions for F¹⁹ in deformed and spherical wells.

²⁸ B. Čujec, Phys. Rev. **136**, B1305 (1964).

ENERGY LEVELS FOR Mg²⁵

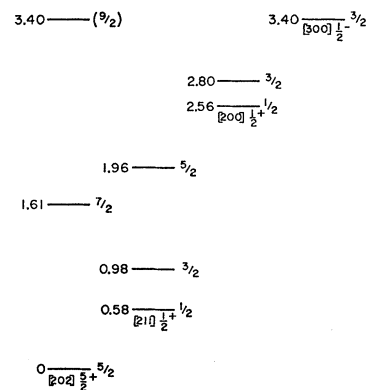


FIG. 7. Energy levels and rotational band structure for Mg²⁵. The 9/2⁺ level at 3.40 MeV was observed in Mg²⁵-(p,p') by G. Crawley [Ph.D. thesis, Princeton University (unpublished)] and is observed in the mirror Al²⁵ nucleus.

²⁹ The DW cross sections are computed in zero range and assume a Hulthén deuteron internal wave function (see Ref. 12).

sitions, since these exist in the model only by coupling between major shells and are thus very sensitive to deformation. The 3.40-MeV $\frac{3}{2}^+$ level (observed in the mirror Al²⁵ nucleus) would agree in order of magnitude with the model if its strength were comparable to the measured 4.06-MeV $\frac{3}{2}^+$ level, since the theoretical predictions (no band mixing) for the latter assuming a $[211]_{\frac{3}{2}}^+$ band are roughly the same. On the other hand, the strength of the $\frac{7}{2}^+$ level at 1.61 MeV is seen to be two orders of magnitude too large and is clearly not the simple stripping of a $g_{7/2}$ neutron. A possible explanation is a second-order $\Delta S=1$ spin-flip process along with the $d_{5/2}$ neutron transfer. Further experimental and theoretical exploration would be interesting since this case is rather unambiguous.

C. Ca⁴⁰(*p,d*)Ca³⁹ and Ca⁴⁰(*d,p*)Ca⁴¹

The Ca isotopes have been extensively studied by stripping³⁰ and pickup³¹ reactions and strong single-particle (hole) levels in Ca⁴¹ (Ca³⁹) are well described by a spherical shell model and a DW analysis.³² On the other hand, weaker low-lying levels of the “wrong” parity have been observed^{33,34} and are very important in determining the extent of collective admixtures in the ground state of Ca⁴⁰. The strongest of these levels are the $\frac{7}{2}^-$ (2.80-MeV) level in Ca³⁹ and the $\frac{3}{2}^+$ (2.02-MeV) level in Ca⁴¹, neither of which fits into a simple shell-model description. If one adopts the viewpoint³⁵ that Ca⁴⁰ is a mixture of spherical and deformed components, one can use the rotational model described above to extract the deformed admixture from the stripping and pickup data. This model is especially convenient for the $d_{3/2}$ stripping since questions of radial nodes (amount of $2d_{3/2}$ in a perturbation expansion) do not arise.

Referring to Fig. 1 and assuming $\beta=0.3$, it is reasonable to assign deformed quantum numbers $\Omega=\frac{3}{2}^+$ for the $d_{3/2}$ stripping and $\Omega=\frac{1}{2}^-$ for the $f_{7/2}$ pickup. The well depths were adjusted with OM-well geometry to fit the binding energies. The results are summarized in Table IV, where the spectroscopic factors are obtained from

$$\begin{aligned} d\sigma/d\Omega &= \frac{3}{2} S\sigma_{\text{DW}}, & (\text{pickup}) \\ d\sigma/d\Omega &= 4S\sigma_{\text{DW}}, & (d_{3/2} \text{ stripping}) \end{aligned} \quad (5.2)$$

the numerical coefficients being statistical weights. A normalized deformed radial wave function is used for

TABLE IV. DW analysis of “unusual” levels in Ca³⁹ and Ca⁴¹.

Nucleus	Ω	lj	B (MeV)	$d\sigma/d\Omega(\theta_{\text{max}})$ (mb/sr)	V (MeV)	$\sigma_{\text{DW}}(\theta_{\text{max}})$ (mb/sr)	S
Ca ³⁹	$\frac{1}{2}^-$	$f_{7/2}$	18.5	0.20	63.0	0.56	0.24
Ca ⁴¹	$\frac{3}{2}^+$	$d_{3/2}$	6.35	0.82	43.0	0.83	0.25

the form factor in σ_{DW} . The OM parameters were taken from elastic-scattering fits³⁶ and are reasonably well known. An examination of the extracted well depths in Table IV indicates a deficiency in the model. Evidently strong “residual” forces are needed to bind a $f_{7/2}$ neutron far below a $d_{3/2}$ neutron. (A deformation $\beta\sim 0.8$ is needed, which seemed a bit absurd.) A better theory of these levels is called for in order to accurately extract a Ca⁴⁰ deformation probability. However, at present the deformed-well model offers a well-defined extraction procedure which is probably an improvement over the usual spherical-well method.

D. Fe⁵⁶(*p,d*)Fe⁵⁵; *j* Dependence

A difference in the 28-MeV (*p,d*) angular distribution between $\frac{7}{2}^-$ and $\frac{5}{2}^-$ states was found by Sherr *et al.*³⁷ in the $A\sim 55$ mass region. The $f_{5/2}$ angular distributions were found to peak at more forward angles than the $f_{7/2}$ distributions and also fall off sharper. The effect could be explained by using a form factor for $f_{5/2}$ with relatively larger tail amplitude and this was achieved artificially by using less binding for $f_{5/2}$ (experimentally the $\frac{5}{2}^-$ and $\frac{7}{2}^-$ levels of Fe⁵⁵ are roughly degenerate) as might be the case if all residual interactions could be switched off.

A preferable procedure to obtain a larger external $f_{5/2}$ form factor is to consider the residual interactions, albeit in a simple approximation. Huby and Hutton,³⁸ using zero-range pairing interactions arrived at a set of coupled equations similar to (3.7) and found an effect in the right direction. An alternative method is to treat the residual interactions as causing an effective nonspherical well, in which case one can employ the formalism already laid out. The values of Ω and β are not well determined but experience showed that an appreciable deformation effect would occur when considerable deformation energy was involved, e.g., the highest $\frac{1}{2}^-$ deformed level in Fig. 1. A typical deformation $\beta=0.3$ was assumed and the effect of deformation on the $f_{5/2}$ component wave function and (*p,d*) pickup cross section is shown in Fig. 8. The well depth using OM parameters was adjusted so the separation energy of the $\Omega=\frac{1}{2}^-$ band agreed with the spheri-

³⁰ T. A. Belote, A. Sperduto, and W. W. Buechner, Phys. Rev. **139**, B80 (1965).

³¹ P. E. Cavanagh, C. F. Coleman, G. A. Gard, B. W. Ridley, and J. F. Turner, Nucl. Phys. **50**, 49 (1964); C. D. Kavaloski, G. Bassani, and N. Hintz, Phys. Rev. **132**, 813 (1963).

³² L. L. Lee, Jr., J. P. Schiffer, B. Zeidman, G. R. Satchler, R. M. Drisko, and R. H. Bassel, Phys. Rev. **136**, B971 (1964).

³³ C. Glashauser, M. Kondo, M. E. Rickey, and E. Rost, Phys. Letters **14**, 113 (1965).

³⁴ R. Bock, H. H. Duhm, and R. Stock, Phys. Letters **18**, 61 (1965).

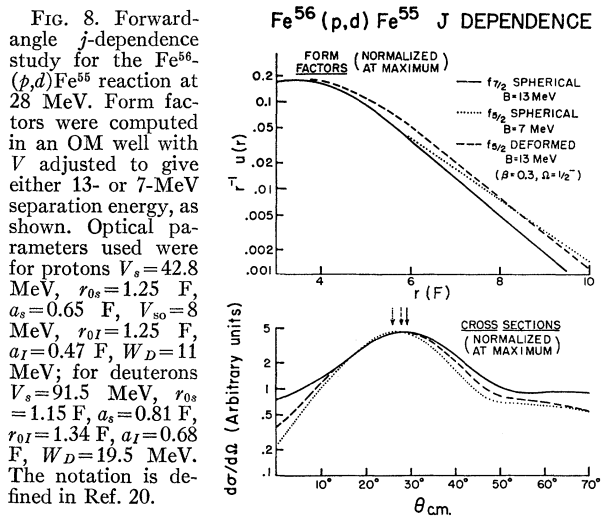
³⁵ W. J. Gerace and A. M. Green (to be published).

³⁶ B. W. Ridley (unpublished). Proton parameters: $V=47.5$ MeV, $r_{0p}=1.15$ F, $a_p=0.70$ F, $V_{s0}=6$ MeV, $r_{0I}=1.252$ F, $a_I=0.75$ F, $W_D=5.4$ MeV; deuteron parameters: $V_s=(83.3+1.023 E_d)$ MeV, $r_{0s}=1.112$ F, $a_s=0.875$ F, $r_{0I}=1.562$ F, $a_I=0.477$ F, $W_D=25.0-0.53 E_D$ MeV. The notation is defined in Ref. 20.

³⁷ R. Sherr, E. Rost, and M. E. Rickey, Phys. Rev. Letters **12**, 420 (1964).

³⁸ R. Huby and J. L. Hutton, Phys. Letters **19**, 660 (1966).

cal $f_{7/2}$ binding energy which was taken to be 13 MeV. Also plotted is the effective-binding prescription where the spherical $f_{5/2}$ level is bound by 7 MeV, i.e., the same spherical well with a reasonable spin-orbit potential. Figure 8 shows that the effect of deformation goes in the same direction as the empirical effective-binding prescription (and the data) but that the effect is too weak. Similar results were found by Huby and Hutton.³⁸ Of course, the parameters of the deformed well, especially Ω and β , are ill determined, as are the optical parameters in the DW analysis, and it may be possible to get agreement by a suitable choice. However, recent work by Glashauser³⁹ suggests that the j -dependent effect is not explainable by any form-factor modifications in the DW analysis, at least at lower energies. Thus the



explanation of forward-angle pickup (as well as backward-angle stripping⁴⁰) j dependence is still largely unknown.

E. Analog States by (p,d)

States of spin $\frac{7}{2}^-$ in nine nuclei with $A \sim 55$ were observed by Sherr *et al.*⁴¹ by means of the (p,d) reaction with 28-MeV protons. In each case the highest $\frac{7}{2}^-$ state seen was found to be the isobaric analog of the lowest $\frac{7}{2}^-$ state of the isobar with one more neutron. Although the angular distributions were in good agreement with DW calculations, the magnitudes of the analog-state transitions were found to be too large compared to the predictions (3.13). Part of the discrepancy could be removed by using improved average

³⁹ C. Glashauser, Ph.D. thesis, Princeton University (unpublished).

⁴⁰ L. L. Lee, Jr., and J. P. Schiffer, Phys. Rev. Letters **12**, 108 (1964); Phys. Rev. **136**, B405 (1964).

⁴¹ R. Sherr, B. F. Bayman, E. Rost, M. E. Rickey, and C. G. Hoot, Phys. Rev. **139**, B1272 (1965).

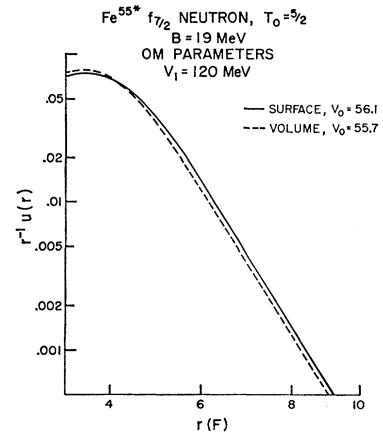


FIG. 9. Analog-state neutron form factors computed with surface and volume coupling terms.

sets^{42,43} of optical parameters. A further enhancement occurs if one employs the coupled-channel approach.

The radial dependence of the coupling term was taken to be of either volume or surface form

$$V_1(r) = V_1 \{1 + \exp[(r - R_0/a)]\}^{-1}, \quad \text{volume} \quad (5.3)$$

$$V_1(r) = -4aV_1 \left[\frac{1}{dr} \frac{d}{dr} \left[\frac{1}{1 + \exp[(r - R_0)/a]} \right] \right], \quad \text{surface}, \quad (5.4)$$

where the parameters $R_0 = r_0 A^{1/3}$ and a are taken to be the same as in the central $V_0(r)$ term. The two forms have the same maximum value V_1 and thus are roughly comparable. The effect of (5.3) and (5.4) on the form factor is shown in Fig. 9, where the depth V_0 of the central well is adjusted slightly to give the experimental separation energy for the $T_0 = \frac{5}{2}$ (analog) $f_{7/2}$ state of Fe^{55} . The surface coupling term is seen to increase the radial wave function in the tail region as already noted by Tamura⁷ and thus increase the (p,d) analog-state cross section by about 40% in this case.

In redoing the DW calculations for the nine nuclei it seemed reasonable to follow the ideas of Pinkston and Satchler¹¹ and keep a fixed central well depth (using the OM parameters), adjusting the radius to fit the

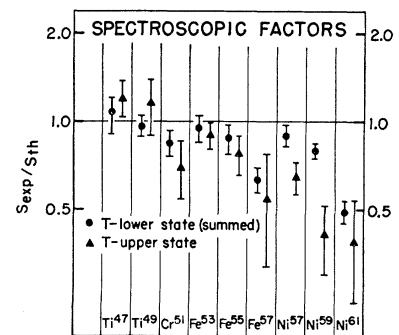


FIG. 10. Comparison of experimental and theoretical values for summed spectroscopic factors for the T -upper analog state and the T -lower configuration state.

⁴² M. P. Fricke and G. R. Satchler, Phys. Rev. **139**, B567 (1965).

⁴³ J. K. Dickens and F. G. Perey, Phys. Rev. **138**, B1083 (1965).

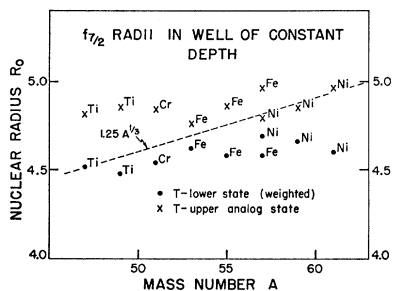


FIG. 11. Potential-well radii R_0 which give $f_{7/2}$ separation energies using OM well parameters $a=0.65$ F, $\Lambda=25$, and $V=55$ MeV plus a surface symmetry-energy term with $V_1=100$ MeV. The T -lower configuration-state energy is taken to be the spectroscopic-factor weighted average.

binding energies. This procedure accurately reproduces the effect of using a symmetry-energy term of surface form (5.4) for different isotopes. Furthermore, the changes in residual interactions, collective or otherwise, between nearby nuclei are probably also of a surface nature.

The confrontation of theory and experimental data³⁷ is displayed in Fig. 10. The DW calculations use average optical parameters^{42,43} and employ local-energy approximations to the effects of finite range⁴⁴ and non-locality.⁴⁵ The over-all agreement with experiment is seen to be satisfactory, the low values for Ni being a possible experimental difficulty in detecting weak $\frac{7}{2}^-$ states.

The potential radii determined by fitting the analog and configuration⁴⁶ $f_{7/2}$ separation energies are shown in Fig. 11. It is seen that the analog radii are 5–10% larger than the corresponding configuration radii and that an approximate constancy in R_0 in the $f_{7/2}$ shell ($A \leq 54$) is observed. These features do not depend sensitively on the parameters in the calculation (e.g., a reasonable volume symmetry-energy term gives the same result). Since the proton component dominates in the coupled system, this result can be interpreted as a larger proton radius than that for a neutron in agreement with the recent work of Soper.⁴⁷

VI. CONCLUSIONS

In the calculations of form factors for nuclear-stripping experiments, it is often necessary to treat nuclear-

⁴⁴ J. K. Dickens, R. M. Drisko, F. G. Perey, and G. R. Satchler, Phys. Letters **15**, 337 (1965). A range of 1.25 F is assumed.

⁴⁵ S. A. Hjorth, J. X. Saladin, and G. R. Satchler, Phys. Rev. **138**, B1425 (1965). A nonlocality parameter $\beta=0.85$ F is assumed for the neutron and proton wells and $\beta=0.54$ F for the deuteron well.

⁴⁶ A spectroscopic-factor weighted configuration energy is used as in Ref. 41.

⁴⁷ J. M. Soper (to be published).

structure effects in more detail than is customary. This is true even if the nuclear interior wave function is irrelevant, e.g., Coulomb stripping or heavy-ion nucleon transfer reactions. The method of coupled channels can often be combined with convenient phenomenological models to obtain more reliable form factors and spectroscopic information.

ACKNOWLEDGMENTS

I wish to acknowledge valuable conversations with B. F. Bayman, R. Sherr, and G. T. Garvey, and especially with G. R. Satchler, who suggested a coupled-channels approach. I am grateful to B. W. Ridley for communicating his results prior to publication. The distorted-wave calculations were performed using the Oak Ridge computer program JULIE, written by R. M. Drisko.

APPENDIX

We outline here the extension of Eq. (3.4) to fourth order in the deformation parameter β . The radius of an equipotential is generalized to fourth order

$$r \rightarrow r_0[1 + \beta Y_2^0(\theta) - \beta^2/4\pi + c_3\beta^3 + c_4\beta^4], \quad (\text{A1})$$

where the constants c_3 and c_4 are determined by applying the constant-volume assumption

$$\int \int r^2 dr d\Omega = \frac{4}{3}\pi r_0^3, \quad (\text{A2})$$

which determines c_3 and c_4 :

$$c_3 = -(1/12\pi)(5/4\pi)^{1/2}(2200|20)^2 \\ = -4.7806 \times 10^{-4}, \quad (\text{A3})$$

$$c_4 = 0.$$

Expanding $V(r_0)$ in a Taylor series as in (3.4) yields the final result

$$V = V(r) + \beta A + \beta^2 B + \beta^3 C + \beta^4 D, \quad (\text{A4})$$

where

$$A = -YV_1, \\ B = Y^2(V_1 + \frac{1}{2}V_2) + (1/4\pi)V_1, \\ C = -Y^3(V_1 + V_2 + \frac{1}{6}V_3) - (1/4\pi)Y(2V_1 + V_2) + c_3V_1, \\ D = Y^4(V_1 + \frac{3}{2}V_2 + \frac{1}{2}V_3 + (1/24)V_4) \\ + (3/4\pi)Y^2(V_1 + V_2 + \frac{1}{6}V_3) \\ + c_3Y(2V_1 + V_2) + (1/(4\pi)^2)(V_1 + \frac{1}{2}V_2).$$

Here Y denotes the spherical harmonic $Y_2^0(\theta, \varphi)$ and $V_n \equiv r^n [d^n V(r)/dr^n]$.